Available online at www.sciencedirect.com
ScienceDirect
Acta Materialia xxx (2008) xxx–xxx
Acta MATERIALIA
www.elsevier.com/locate/actamat

Effects of pre-strain on the compressive stress–strain response of Mo-alloy single-crystal micropillars

H. Bei [a,*], S. Shim [a,b], G.M. Pharr [a,b], E.P. George [a,b]

[a] *Materials Science and Technology Division, Oak Ridge National Laboratory, Oak Ridge, TN 37831, USA*
[b] *Department of Materials Science and Engineering, University of Tennessee, Knoxville, TN 37996, USA*

Received 20 February 2008; received in revised form 14 May 2008; accepted 14 May 2008

Abstract

A NiAl–Mo eutectic was directionally solidified to produce composites with well-aligned single-crystal Mo-alloy fibers embedded in a NiAl matrix. They were pre-strained by compressing along the fiber axis and then the matrix was etched away to expose free-standing micropillars having different sizes (360–1400 nm) and different amounts of pre-strain (0–11%). Compression testing of the pillars revealed a variety of behaviors. At one extreme were the as-grown pillars (0% pre-strain) which behaved like dislocation-free materials, with yield stresses approaching the theoretical strength, independent of pillar size. At the other extreme were pillars pre-strained 11% which behaved like the bulk, with reproducible stress–strain curves, relatively low yield strengths, stable work-hardening and no size dependence. At intermediate pre-strains (4–8%), the stress–strain curves were stochastic and exhibited considerable scatter in strength. This scatter decreased with increasing pre-strain and pillar size, suggesting a transition from discrete to collective dislocation behavior.

Keywords: Plastic deformation; Yield phenomena; Crystal plasticity; Size dependence; Mechanical properties

1. Introduction

In many cases one needs to be able to measure and understand the mechanical behavior of small volumes of materials including, for example, microelectronic devices and components that have shrunk in size to submicrometer dimensions and structural materials in which the constituent phases can have length scales of a few nanometers to hundreds of nanometers. It is also sometimes necessary to know how mechanical properties vary from point to point in a complex structural component in order to understand both how properties evolved from prior processing and to predict future service behavior. To accomplish this, spatially resolved mechanical tests can be performed in situ, e.g., by micro/nanoindentation [1], or ex situ by micromachining small-scale specimens from the regions of interest and conducting microcompression/tensile tests [2]. Regardless of the manner in which the tests are performed, it is important to understand how the measured mechanical properties are influenced by the small length scales of the tested materials (i.e., sample size effects).

Sample size effects can be due to the specific specimen preparation technique or testing method employed. For example, the measured hardness of a thin film is often influenced by the hardness of the substrate and the residual stress in the thin film, because measurement of hardness normally requires that the film be attached to a substrate [3–6]. Mechanical properties can also be influenced by the additional strengthening imparted by the geometrically necessary dislocations [7,8] needed to accommodate the plastic strain gradients that are unavoidable in certain test geometries, e.g., in indentation, [9–11] microbending [12] and microtorsion [13].

Recently, a new microcompression test was developed to measure the small-scale mechanical behavior of free-standing pillars [14,15]. Using this method, micropillars with

* Corresponding author. Tel.: +1 865 5767196; fax: +1 865 5747659.
E-mail address: Beih@ornl.gov (H. Bei).

1359-6454/$34.00 © 2008 Acta Materialia Inc. Published by Elsevier Ltd. All rights reserved.
doi:10.1016/j.actamat.2008.05.030

sizes down to a few hundred nanometers have been fabricated and tested in compression [14–24]. The compression testing is typically conducted in a modified nanoindentation system equipped with a flat-tip indenter and, as in the case of bulk compression tests, is believed to largely avoid strain gradient effects, although recent tensile tests on long-gage-length specimens [25] suggest that end effects can influence the measured strengths. Several methods can be used to fabricate micropillars for compression testing [14–24], but the most common technique is fabrication from bulk materials by focused ion beam (FIB) milling [14–23].

A potential drawback of FIB milling is that it may introduce extrinsic defects into a layer adjacent to the milled surface. These defects include implanted Ga ions, dislocations, intermetallic compounds and near-surface amorphous layers [26–30], which can potentially confuse the interpretation of intrinsic mechanical behavior, especially at small size scales [27,31]. The dislocation density after FIB milling can be high ($\sim 10^{15}$ m^{-2}), [32] but there is evidence to suggest that it decreases during subsequent compression [32]. The reduction occurs more effectively in smaller (160 nm) pillars than in larger (290 nm) pillars [32].

Recently, we developed an alternative technique to produce single-crystal micropillars that avoids FIB milling altogether. Our technique involves directional solidification of eutectic alloys to produce long-aspect-ratio fibrous composites followed by etching away of the matrix to expose the fibers as free-standing micropillars [24]. Compression tests of single-crystal Mo-alloy micropillars produced in this way showed that, after an initial elastic regime, they all yielded at shear stresses close to the theoretical, independent of size, for sizes in the range 360–1000 nm [24]. In other words, the Mo-alloy micropillars produced using our directional solidification technique behaved like dislocation-free materials [33,34].

Pillars produced by directional solidification offer a unique opportunity to investigate small-scale mechanical behavior because we can systematically introduce dislocations by room temperature pre-straining to study the effects of initial dislocation structure on pillar behavior without the confounding effects of other defects that may be present in FIB-milled pillars. Here, we present our initial results on the effects of pre-strain on body-centered cubic (bcc)-structured Mo-alloy pillars of varying sizes.

2. Materials and methods

2.1. Sample preparation

Starting with the elemental constituents (Ni, Al and Mo, all >99.99% pure), eutectic alloys having the composition Ni–45.5Al–9Mo (at.%) were arc melted and drop-cast into a cylindrical copper mold measuring 10 mm in diameter and 100 mm in length. The drop-cast alloys were directionally solidified in a high-temperature optical floating zone furnace in flowing argon gas to produce well-aligned fibrous composites consisting of [1 0 0] oriented Mo-alloy fibers with approximately square cross-sections embedded in a NiAl matrix. Details of the growth, microstructural characterization and mechanical properties of these composites are given elsewhere [35].

Although the fibers in the eutectic composite are actually Mo solid solutions (86Mo–10Al–4Ni, at.%), we will refer to them simply as "Mo fibers" or "Mo pillars". Also, when we refer to the size of the Mo fibers or pillars, what we mean is the edge length (a) of their square cross-sections. This dimension was obtained by measuring the cross-sectional area (A) of the fibers using image analysis software and assuming that $a = \sqrt{A}$. The Mo fiber size was shown previously [35] to be inversely proportional to the square root of the directional solidification rate, R, which allowed us to obtain fiber sizes ranging from ~360 to 1400 nm by adjusting R between 5 and 80 mm h^{-1}. The as-grown fibers are long and have fairly uniform cross-sections over their entire lengths, as shown in Fig. 1, where the matrix has been etched away to reveal the fibers.

The directionally solidified composites were cut transversely into 2 mm thick disks (i.e., perpendicular to the growth direction) by electric-discharge machining. Some of the disks were pre-strained at room temperature by compression normal to their axes (i.e., parallel to the fiber axes). The amount of imposed engineering pre-strain (percentage thickness reduction) ranged from 0% to 11%.

The as-grown and pre-strained disks were mounted in epoxy, and ground/polished using standard metallographic procedures. The final polishing step was carried out in an automatic vibratory polishing machine with colloidal silica as the polishing medium. The polished samples were etched in a solution of 74% H_2O, 18% HCl and 8% H_2O_2 to remove the NiAl matrix and expose the fibers as free-standing Mo pillars. The matrix etched away at a rate of approximately 1 μm min^{-1} which allowed us to control the aspect ratios of the Mo pillars within the range 2.5–3.0. The etched specimens were examined in a scanning electron

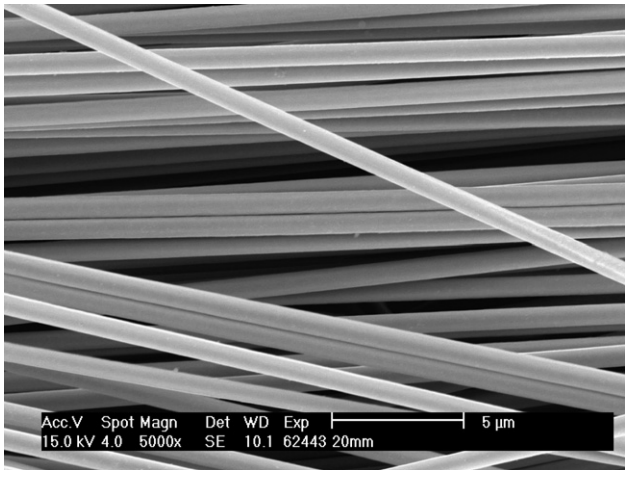

Fig. 1. As-grown (directionally solidified) Mo fibers after complete removal from the NiAl matrix by selective etching.

Please cite this article in press as: Bei H et al., Effects of pre-strain on the compressive stress–strain response ..., Acta Mater (2008), doi:10.1016/j.actamat.2008.05.030

microscope (SEM) to determine the quality of the pillars and measure their dimensions.

2.2. Microcompression tests

The mechanical response of the Mo pillars was investigated in uniaxial compression with a Nanoindenter XP® [24]. Cube-corner pyramidal diamond indenters were FIB-milled to produce cylindrical flat punch tips. An example of one such tip having a nominal diameter of 2.2 μm is shown in Fig. 2. Three different tips with nominal diameters of 4.5, 2.2 and 0.8 μm were fabricated for compression of the different size pillars. They were chosen to have diameters larger than the pillars but radii smaller than the pillar spacing, so as to act as effective compression platens without interference from the surrounding pillars.

The experiments were run in load control at a constant loading rate (dP/dt) in the range 5–25 nN s^{-1} (scaled for pillar size) to a prescribed maximum displacement of ~20% of the pillar height, resulting in an initial strain rate of $\sim 10^{-4}$ s^{-1} for all the tests. Compression tests were conducted in 14 × 14 arrays (i.e., at 196 individual locations on each sample) with a spacing of 5–10 μm between test locations. After compression, the samples were photographed in a SEM. Several of the locations at which compression tests were conducted coincided with pillar locations. However, the cylindrical flat punch indenter landed squarely on only a few of the pillars; in other cases, the indenter compressed only a portion of the pillar or compressed adjacent pillars simultaneously, as discussed in an earlier paper [24]. By careful examination of the SEM images, the former were isolated and classified as valid compression tests. For the larger sizes ($a > 600$ nm), the actual pillars associated with the valid compression tests were identified in the SEM images taken before compression and their cross-sectional areas measured using image analysis software. For the smaller pillars ($a < 600$ nm), the areas of the actual pillars that were compressed were not measured; rather, an average area was used that was obtained by measuring the areas of more than 36 randomly selected pillars in a region of the sample where the compression tests were conducted. This procedure is slightly different from that used in our earlier paper [24] where pillars with sizes down to ~500 nm were individually tracked and average areas were used only for pillars smaller than 500 nm. Engineering stress–strain curves were obtained by dividing the load and displacement data by the initial cross-sectional areas and heights of the pillars.

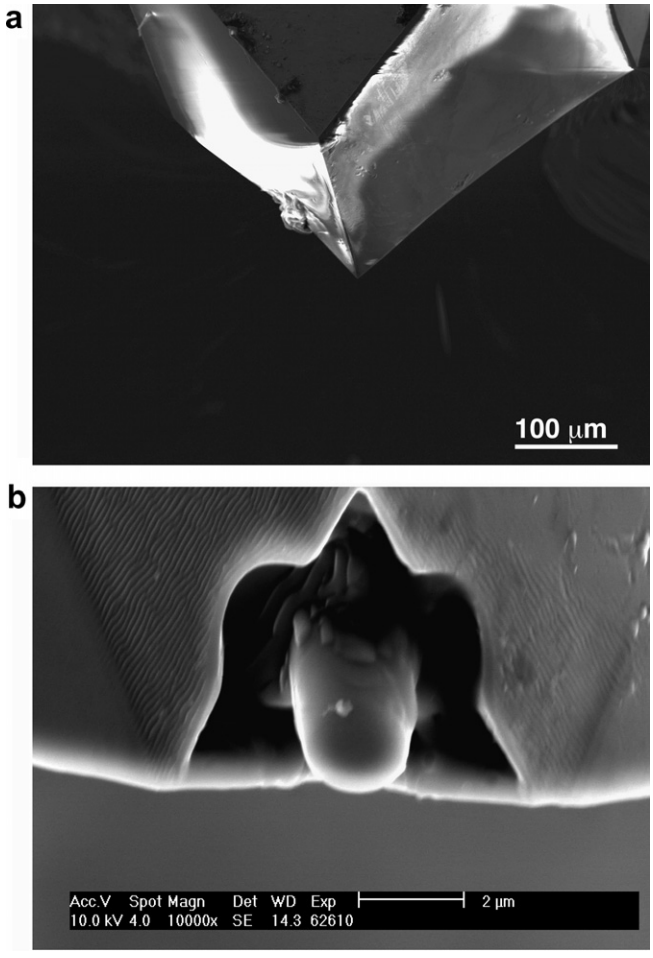

Fig. 2. SEM images of (a) a cube-corner diamond indenter used to fabricate (b) a cylindrical flat punch indenter with a diameter of ~2.2 μm by focused ion beam milling.

3. Results

3.1. Pre-strain effects on the deformation behavior of 500–550 nm micropillars

For the as-grown Mo pillars (0% pre-strain), the key findings have been reported previously [24]. However, to put the new results of this study in context, we briefly describe some of those earlier results first. The as-grown pillars exhibited reproducible engineering stress–strain curves (see examples in Fig. 3) that are initially linear elastic but, upon reaching a high critical stress of 9.3 ± 0.5 GPa, yield with a sudden strain burst corresponding to catastrophic plastic collapse. Stable plastic flow was not observed in any of the 12 pillars tested and, once plasticity commenced, it continued catastrophically. This phenomenon is similar to that observed in tensile tests of metal whiskers by Brenner [33,34], suggesting that there is significant strain softening after yielding. However, the degree of strain softening and how plasticity takes place cannot be recorded because the nanoindentation system used for the compression tests is load-controlled. Scanning electron micrographs taken after the compression tests showed that all the pillars collapsed to form pancakes of deformed material (Fig. 3b,c), indicating that severe plastic deformation occurs in the pillars. The critical resolved shear stress for the $(1\,1\,2)$ $[11\bar{1}]$ slip system of these bcc pillars was determined to be ~4.6 GPa [24], or ~1/25 of the shear modulus, which is within the range expected for theoretical shear strengths [33,34].

Please cite this article in press as: Bei H et al., Effects of pre-strain on the compressive stress–strain response ..., Acta Mater (2008), doi:10.1016/j.actamat.2008.05.030

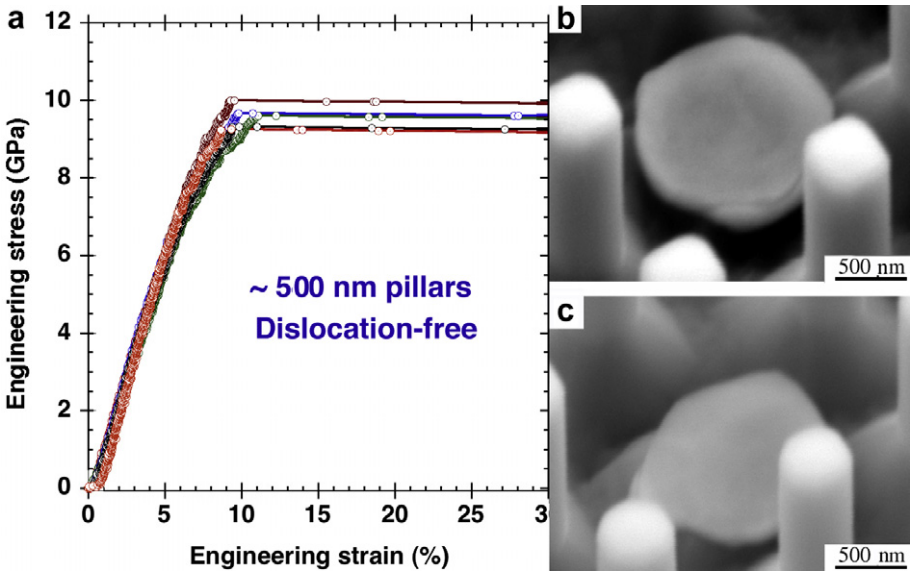

Fig. 3. Results of compression tests of ~500 nm Mo pillars in the as-grown condition: (a) engineering stress–strain curves showing yielding at very high stresses followed by sudden large strain bursts and (b,c) SEM images of pillars after compression tests showing catastrophic plastic collapse.

In sharp contrast to the unstable plasticity observed in as-grown pillars, stable plastic flow, similar to that expected in "bulk" samples, can be achieved in ~550 nm pillars if they are given a 11% pre-strain prior to testing (Fig. 4). The engineering stress–strain curves show continuous strain hardening, with a 0.2% offset yield stress of 1.00 ± 0.08 GPa, which is almost an order of magnitude lower than that of the as-grown pillars (~9.3 GPa). Together, these results are consistent with the view that, in dislocation-free materials, yielding occurs at a very high stress because dislocations have to be first nucleated at the theoretical stress [36–38], whereas, in materials containing pre-existing dislocations, yielding occurs at a significantly lower stress by the movement or unlocking of pre-existing dislocations [37,38].

Unlike the 0% pre-strained pillars (Fig. 3b,c), the 11% pre-strained pillars (Fig. 4b,c) do not collapse uncontrollably. Rather, because they yield at a relatively low stress and then work harden in a stable way, the load-controlled nanoindentation system is able to stop the test after the prescribed 20% strain. After compression, at least one major slip offset can be seen on the pillar surfaces (see Fig. 4b,c).

We also investigated the behavior of pillars after intermediate pre-strains of 4–8%, and found significantly different features in their deformation behavior. Fig. 5 shows several stress–strain curves of ~550 nm pillars given a 4%

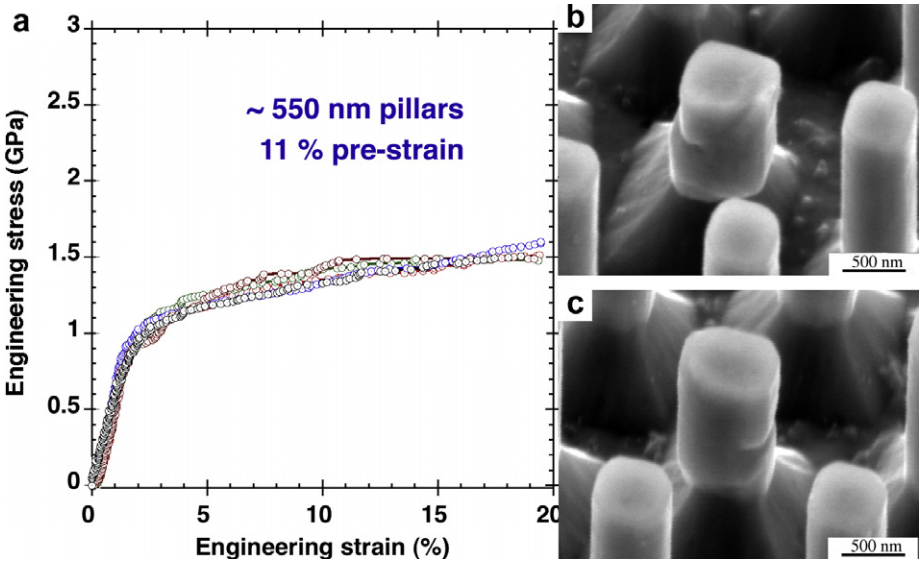

Fig. 4. Results of compression tests of ~550 nm pillars after 11% pre-strain: (a) engineering stress–strain curves showing "bulk-like" behavior with low yield stresses and normal strain hardening and (b,c) SEM images of pillars after compression.

Please cite this article in press as: Bei H et al., Effects of pre-strain on the compressive stress–strain response ..., Acta Mater (2008), doi:10.1016/j.actamat.2008.05.030

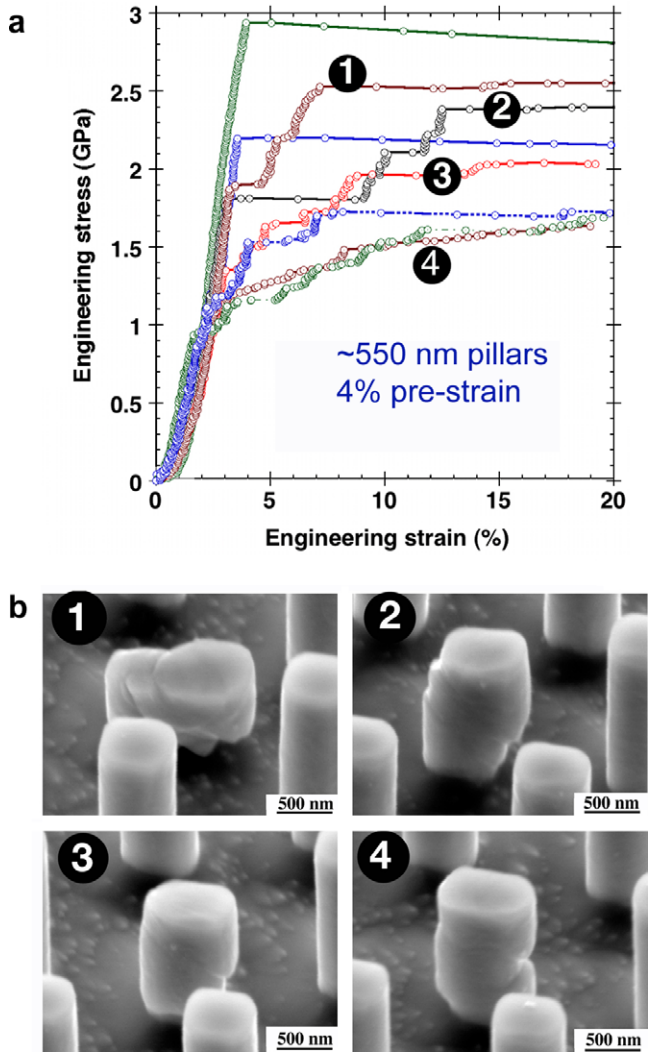

Fig. 5. Results of compression tests of ~550 nm pillars after 4% pre-strain: (a) engineering stress–strain curves showing a variety of deformation behaviors and (b) SEM images of pillars after compression. The numbers indicate which pillar corresponds to which stress–strain curve.

pre-strain. As can be seen, some of the pillars (e.g. pillar 4) show relatively stable stress–strain behavior, similar to that observed in the 11% pre-strained pillars. After compression, pillar 4 showed evidence of two non-parallel slip bands that were active during deformation. The lower one appears to have been constrained at the bottom, which may have led to the activation of a second, differently oriented slip band at a different location in the gage section. However, without in situ examination during deformation it is impossible to know for sure which one became active first. Other pillars (e.g. those labeled 1–3 in Fig. 5) exhibited jerky flow and "stair-step" shaped stress–strain curves similar to what has been reported in the case of FIB-milled pillars [e.g., 14]. When examined after compression, these pillars showed evidence of multiple, parallel slip bands. Still other pillars (e.g., 14 the topmost curve in Fig. 5a) exhibited behavior that is reminiscent of the unstable plasticity seen in as-grown pillars (Fig. 3), but without their high strength. It should be noted that all the 4% pre-strained pillars (total of 15 tested) had yield strengths that are substantially lower than those of the as-grown pillars.

Broadly similar behavior was observed in the ~550 nm pillars given a pre-strain of 8% (Fig. 6). However, the scatter in strengths was found to be less than that for the 4% pre-strained pillars (cf. Fig. 5a). In both the 4% and 8% pre-strained pillars the lowest yield strengths observed were approximately the same (~0.9 GPa). However, the highest yield strength achieved in the 8% pre-strained pillars (1.73 GPa) was lower than that of the 4% pre-strained pillars (2.90 GPa). The measured yield strengths of the various Mo pillars with different amounts of pre-strain are listed in Table 1.

Fig. 7 summarizes the effects of pre-strain on the yield strengths of the 500–550 nm pillars. The yield strength decreases with increasing pre-strain from approximately the theoretical strength (~9.3 GPa) for the as-grown pillars (0% pre-strain) to ~1.00 GPa for the 11% pre-strained pillars. As mentioned before, the yield strengths of the as-grown and the 11% pre-strained pillars exhibit relatively small scatter (standard deviations of ±8% of the mean values), whereas, the yield strengths of the 4% and 8% pre-strained pillars show large scatter (standard deviations of 37% and 17% of the mean values for 4% and 8% pre-strained pillars, respectively). For pre-strains greater than 4%, the magnitude of the scatter decreases with increasing pre-strain.

3.2. Sample size effects on strengths of micropillars

We showed in an earlier paper [24] that pillar size (in the range 360–1000 nm) does not affect the yield strength of as-grown pillars (0% pre-strain). They all behaved like dislocation-free materials, with reproducible stress–strain curves

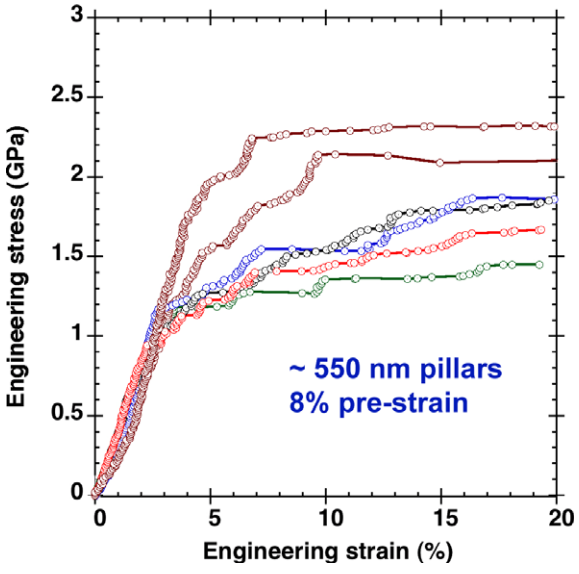

Fig. 6. Engineering stress–strain curves of ~550 nm pillars after 8% pre-strain showing a variety of deformation behaviors.

Please cite this article in press as: Bei H et al., Effects of pre-strain on the compressive stress–strain response ..., Acta Mater (2008), doi:10.1016/j.actamat.2008.05.030

Table 1
Compressive yield strengths of 500–550 nm Mo pillars given different amounts of pre-strain

Pre-strain (%)	No. of valid tests	Yield strength (GPa)	Average yield strength (GPa)
4	15	2.90, 2.19, 1.87. 1.81, 1.36, 1.17, 0.96, 1.12, 2.53, 2.00, 1.49, 1.29, 1.25, 1.14, 0.95	1.61 ± 0.60
8	10	1.38, 0.92, 1.24, 1.53, 1.18, 1.17, 1.23, 1.41, 1.27, 1.73	1.30 ± 0.22
11	12	0.97, 1.14, 0.92, 1.12, 0.90, 0.91, 1.11, 1.06, 0.93, 0.95, 0.96, 1.06	1.00 ± 0.09

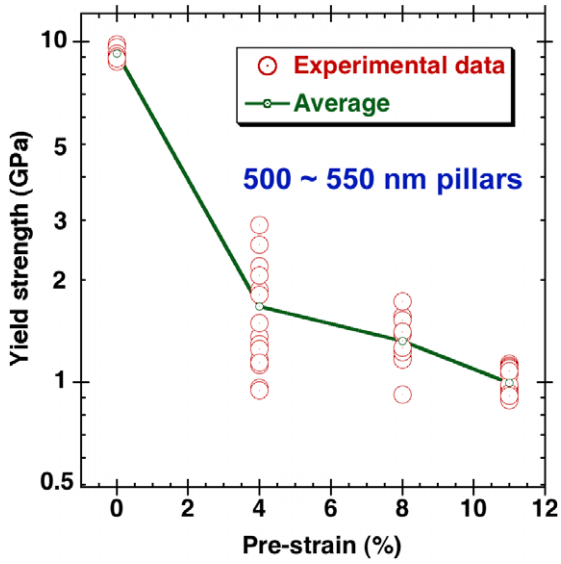

Fig. 7. Yield strengths of 500–550 nm pillars as a function of pre-strain. Note the relatively high scatter at intermediate pre-strains (4% and 8%).

that exhibited an initial elastic region followed by yielding and plastic collapse at the theoretical strength, independent of size. Here, we investigate how sample size affects the behavior of pre-strained pillars. For this we first focus on those pillars that exhibit stable plastic deformation (i.e., those subjected to 11% pre-strain). Fig. 8 shows typical stress–strain curves of the large 1400 nm pillars. These curves are similar to those of the ~550 nm pillars (Fig. 4), suggesting a minimal effect of pillar size on strength. A systemic analysis was conducted of the mechanical response after 11% pre-strain for pillar sizes in the range ~360–1500 nm. As shown in Fig. 9, no pillar size effects are seen for either the 0.2% offset yield stress, or the 5% and 15% flow stresses. Therefore, at the two extremes of pre-strain investigated (0% and 11%), there is no size effect on the strengths of the Mo pillars.

Next, we examine the effect of pillar size for 4% pre-strain (i.e., between the above two extremes). Relatively small pillars (~550 nm) behave in a stochastic manner, as mentioned earlier (Fig. 5a). In contrast, big pillars (~1200 nm) have smoother stress–strain curves with more stable work-hardening, as shown in Fig. 10. In general, the bigger pillars have less jerky and more reproducible stress–strain curves (i.e. they exhibit less scatter). The lowest strengths observed are comparable for the two pillar sizes but there are more of the ~550 nm pillars with higher strengths than the ~1200 nm pillars. Based on the results of 15 tests performed for each pillar size, the average yield stress for the smaller (~550 nm) pillars was determined to be 1.61 ± 0.6 GPa and for the larger pillars (~1200 nm)

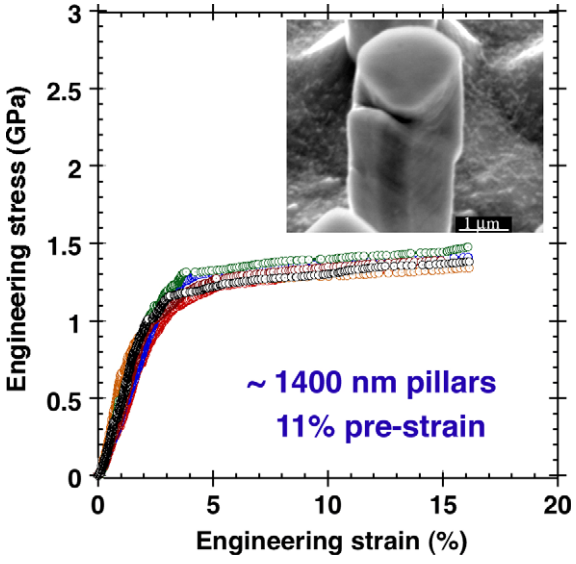

Fig. 8. Engineering stress–strain curves of ~1400 nm pillars after 11% pre-strain showing "bulk-like" behavior with low yield stresses and normal strain hardening behavior. Inset is a SEM image of a pillar after compression.

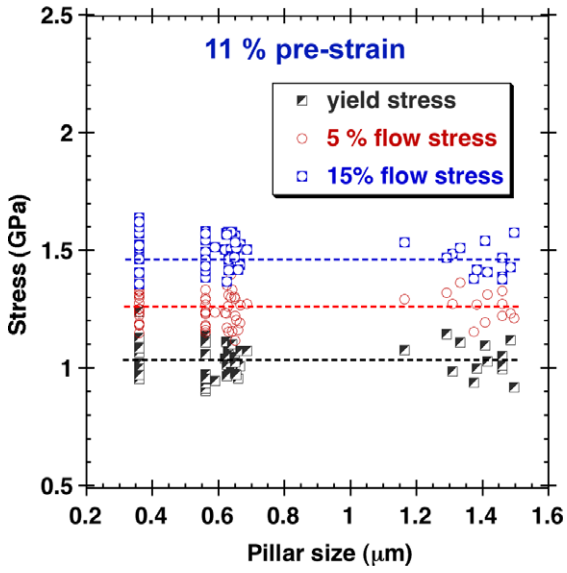

Fig. 9. Dependence of the 0.2% offset yield stress, and the 5% and 15% flow stresses, on pillar size for Mo pillars given a 11% pre-strain.

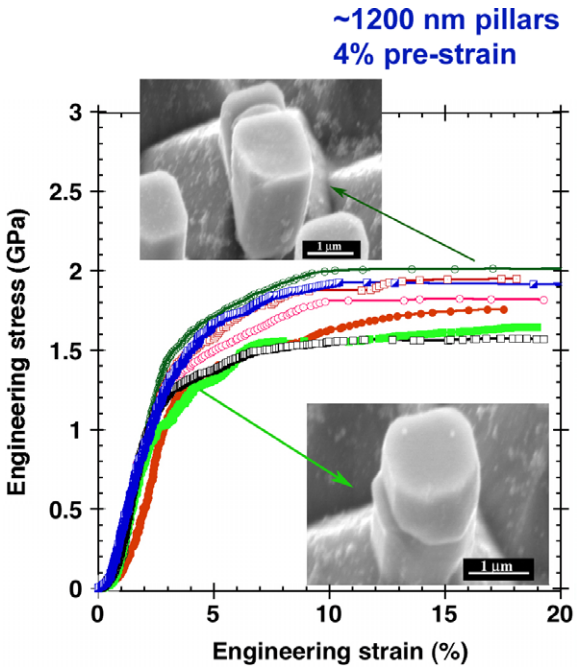

Fig. 10. Engineering stress–strain curves of ~1200 nm pillars after 4% pre-strain. Insets are SEM images of pillars after compression.

1.32 ± 0.2 GPa. An interesting similarity is revealed between size and pre-strain effects if one compares Figs. 5a and 10 on the one hand, and Figs. 5a and 4 on the other: the stress–strain curves become more reproducible (and "bulk-like") with increasing pillar size (for a fixed amount of pre-strain) and increasing pre-strain (for a fixed pillar size).

4. Discussion

Fig. 11a summarizes our results for the dependence of yield strength on pillar size and pre-strain. At one extreme, the data for the 0% pre-strained specimens (360–1000 nm) represent an upper bound corresponding to the theoretical strength. This is consistent with transmission electron microscopy results which have shown that the Mo fibers in directionally solidified NiAl–Mo eutectics are dislocation-free [39]. They are also consistent with the whisker test results reported by Brenner many years ago [33,34].

At the other extreme, the data for the 11% pre-strained pillars appear to represent a lower bound, corresponding to behavior that may be expected of the "bulk". This view is given credence by the stress–strain curves shown in Fig. 4, which look like bulk curves even though they are actually for relatively small ~550 nm pillars. The way to confirm this, of course, is by performing compression tests on bulk single-crystals having the same orientation and composition as our Mo pillars (Mo–10Al–4Ni, at.%). Unfortunately, when we tried to grow a single-crystal of this composition [35], the large difference in the melting points of Mo and Al made it impossible for us to prevent large-scale evaporation of Al (in fact, the boiling point of Al, 2450 °C, is lower than the melting point of Mo, 2610 °C).

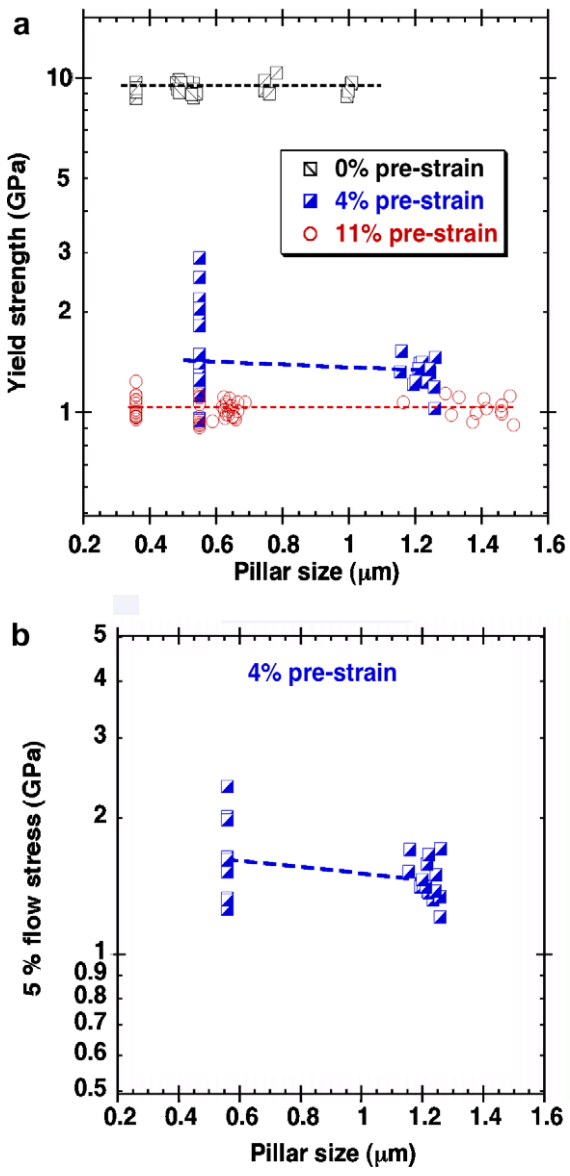

Fig. 11. Dependence of (a) yield strength, and (b) flow stress on pillar size for different pre-strains.

At both the upper and lower extremes, strength is independent of pillar size, but for different reasons. The upper bound is related to the stress needed for dislocation nucleation which is the same for all pillar sizes. It is conceivable that for much larger sizes than those shown in Fig. 10, one might encounter a sufficient number of mobile dislocations even in directionally solidified pillars. But for the size range investigated so far, the as-grown pillars behave like dislocation-free materials and their yield strength is given by the size-independent theoretical strength. At the lower bound the situation is different because a significant number of dislocations might be already present in the pillars as a result of the 11% pre-strain. Therefore, they do not have to be nucleated and the yield/flow stresses are governed

Please cite this article in press as: Bei H et al., Effects of pre-strain on the compressive stress–strain response ..., Acta Mater (2008), doi:10.1016/j.actamat.2008.05.030

by their collective motion and interaction. If a sufficiently large number of dislocations are introduced, the effects of individual dislocations would "average out" and one would not expect any size effect, as in bulk crystals. This seems to be the case for the 11% pre-strained pillars; however, detailed analyses of the dislocation substructures are needed before any definitive conclusions can be made.

At intermediate pre-strains, the variability in the dislocation distribution from pillar to pillar results in a variety of observed stress–strain behaviors. This stochastic behavior is expected to dominate when the average dislocation spacing approaches the specimen dimensions. Consistent with this view, for a fixed pre-strain of 4%, the scatter in the measured yield strengths is smaller for the bigger pillars (Fig. 10). If we assume that a given amount of pre-strain results in a fixed dislocation density, and, therefore, a fixed dislocation spacing, it stands to reason that the smaller pillars would exhibit more scatter. A similar trend has been reported by Uchic et al. [14], although their pillars were not intentionally pre-strained but contained pre-existing dislocations from processing. Recent discrete dislocation simulations also show increasing scatter with decreasing pillar size for a fixed dislocation density [40]. In addition to the above specimen size effects, we show here that, for pre-strains in the range 4–11%, the yield strength scatter decreases with increasing amounts of pre-strain (Fig. 7). Both these trends can be rationalized if we assume that the probability of finding mobile dislocations in the tested volume increases with increasing specimen size (for a given dislocation density), and increasing dislocation density/pre-strain (for a given specimen size).

In principle, there should be size-dependent strengthening associated with the transition from bulk to ideal (theoretical) strength. For the results shown in Fig. 11a, therefore, one would expect a size effect to be manifested at intermediate pre-strains. Consistent with this view, the limited data available for the 4% pre-strained pillars suggest that the average yield stress of the smaller pillars is ~22% higher than that of the larger pillars. However, it must be noted that there is considerable scatter in the strengths of the smaller pillars (standard deviation of ±38% of the mean value). Therefore, additional experiments are needed to improve the statistics in the intermediate pre-strain regime. Meanwhile, we can also evaluate how the 5% flow stress varies with pillar size for the 4% pre-strained samples, as shown in Fig. 11b. For this exercise, we did not include any data from pillars that showed unstable flow after yielding (single pop-in with no intervening hardening events). Our reasoning was that, in a load-controlled experiment, it is impossible to know what the flow behavior is during an unstable pop-in event. Nevertheless, such exclusion biases the data shown in Fig. 11b to 550 nm pillars that on average have lower yield stresses. Whether it also results in a bias towards lower flow stresses cannot be determined since, as mentioned above, there is no way to know the relationship of the 5% flow stress to the yield stress (it could well be lower if there is a large yield drop). With these caveats noted, the average flow stress for the ~550 nm pillars is 1.60 ± 0.6 GPa, and that for the ~1200 nm pillars is 1.46 ± 0.2 GPa. Therefore, the smaller pillars are again stronger (by ~10%) but also exhibit more scatter (±38% of the mean value).

5. Summary

We investigated the effects of pre-existing dislocations on the mechanical response of single-crystal Mo-alloy micropillars using compression tests. The pillars ranged in size from ~360 to ~1500 nm and were produced by etching away the NiAl matrix in directionally solidified NiAl–Mo fibrous composites. Dislocations were introduced into the micropillars before compression testing by pre-straining the composites at room temperature to various amounts. The NiAl matrix was then etched away to reveal free-standing Mo pillars having different sizes and different amounts of pre-strain. Stable plastic deformation (bulk-like behavior) can be achieved even in pillars as small as ~360 nm provided that enough pre-strain (~11%) is given. The yield and flow strengths of pillars given this amount of pre-strain are independent of sample size in the range 360–1500 nm. For pillars given lower pre-strains (4–8%), the strengths and stress–strain curves show considerable scatter, with the scatter increasing as the pillar size decreases and the pre-strain decreases. Pillars tested in the as-grown condition (i.e., without any pre-strain) behave like dislocation-free materials and yield, independent of size, at very high stresses, approaching the theoretical strength.

Acknowledgements

This research was sponsored by the US Department of Energy: Division of Materials Sciences and Engineering (H.B. and E.P.G.); the Assistant Secretary for Energy Efficiency and Renewable Energy, Office of FreedomCAR and Vehicle Technologies, as part of the High Temperature Materials Laboratory User Program (S.S.); and the SHaRE User Facility, Division of Scientific User Facilities, Office of Science (G.M.P.).

References

[1] Oliver WC, Pharr GM. J Mater Res 1992;7:1564–83.
[2] Uchic MD, Dimiduk DM. Mater Sci Eng A 2005;400:268–78.
[3] Pharr GM, Oliver WC. MRS Bull 1992;17:28–33.
[4] Tsui TY, Pharr GM. J Mater Res 1999;14:292–301.
[5] Nix WD. Metall Trans A 1989;20:2217–45.
[6] Kraft O, Volkert CA. Adv Eng Mater 2001;3:99–110.
[7] Ashby MF. Philos Mag 1970;2:1399–424.
[8] Gao H, Huang Y, Nix WD, Hutchinson JW. J Mech Phys Solids 1999;47:1239–63.
[9] McElhaney KW, Vlassak JJ, Nix WD. J Mater Res 1998;13:1300–6.
[10] Nix WD, Gao HJ. J Mech Phys Solids 1998;46:411–25.
[11] Swadener JG, George EP, Pharr GM. J Mech Phys Solids 2002;50:681–94.
[12] Stolken JS, Evans AG. Acta Mater 1998;46:5109–15.

[13] Fleck NA, Muller GM, Ashby MF, Hutchinson JW. Acta Metall Mater 1994;42:475–87.
[14] Uchic MD, Dimiduk DM, Florando JN, Nix WD. Science 2004;305:986–9.
[15] Dimiduk DM, Uchic MD, Parthasarathy TA. Acta Mater 2005;53:4065–77.
[16] Greer JR, Nix WD. Phys Rev B 2006;73:245410.
[17] Greer JR, Oliver WC, Nix WD. Acta Mater 2005;53:1821–30.
[18] Greer JR, Oliver WC, Nix WD. Acta Mater 2006;54:1705.
[19] Dimiduk DM, Woodward C, LeSar R, Uchic MD. Science 2006;312:1188–90.
[20] Volkert CA, Lilleodden ET. Philos Mag 2006;86:5567–79.
[21] Schuster BE, Wei Q, Zhang H, Ramesh KT. Appl Phys Lett 2006;88:103112.
[22] Uchic MD, Dimiduk DM, Wheeler R, Shade PA, Fraser HL. Scripta Mater 2006;54:759–64.
[23] Ng KS, Ngan AHW. Acta Mater 2008;56:1712–20.
[24] Bei H, Shim S, George EP, Miller MK, Herbert EG, Pharr GM. Scripta Mater 2007;57:397–400.
[25] Kiener D, Grosinger W, Dehm G, Pippan R. Acta Mater 2008;56:580–92.
[26] McCaffrey JP, Phaneuf MW, Madsen LD. Ultramicroscopy 2001;87:97–104.
[27] Kiener D, Motz C, Rester M, Jenko M, Dehm G. Mater Sci Eng A 2007;459:262–72.
[28] Thompson K et al. Ultramicroscopy 2007;107:131.
[29] Maass R et al. Appl Phys Lett 2006;89:51905.
[30] Mayer J, Giannuzzi LA, Kamino T, Michael J. MRS Bull 2007;32:400.
[31] Bei H, Shim S, Miller MK, Pharr GM, George EP. Appl Phys Lett 2007;91:111915.
[32] Shan ZW, Mishra RK, Asif SAS, Warren OL, Minor AM. Nat Mat 2008;7:115–9.
[33] Brenner SS. J Appl Phys 1956;27:1484–956.
[34] Brenner SS. J Appl Phys 1957;28:1023–6.
[35] Bei H, George EP. Acta Mater 2005;53:69–77.
[36] Bei H, Gao YF, Shim S, George EP, Pharr GM. Phys Rev B 2008;77:060103. R.
[37] Cottrell AH. Dislocations and Plastic Flow in Crystals. Oxford: Clarendon Press; 1953.
[38] Honeycombe RWK. Plastic Deformation of Metals. London: Edward Arnold; 1984.
[39] Misra A, Wu ZL, Kush MT, Gibala R. Philos Mag A 1998;78:533–50.
[40] Senger J, Weygand D, Gumbsch P, Kraft O. Scripta Mater 2008;58:587–90.

Please cite this article in press as: Bei H et al., Effects of pre-strain on the compressive stress–strain response ..., Acta Mater (2008), doi:10.1016/j.actamat.2008.05.030